Published in final edited form as:
Nanoscale. 2013 November 7; 5(21): . doi:10.1039/c3nr00908d.

Modulation of Hydrogel Nanoparticle Intracellular Trafficking by Multivalent Surface Engineering with Tumor Targeting Peptide†

Leshern Karamchand[a,‡], **Gwangseong Kim**[a,‡], **Shouyan Wang**[a], **Hoe Jin Hah**[a], **Aniruddha Ray**[a], **Ruba Jiddou**[a], **Yong-Eun Koo Lee**[a], **Martin A. Philbert**[b], and **Raoul Kopelman**[a]

Raoul Kopelman: kopelman@umich.edu

[a]930 North University Ave., Department of Chemistry, University of Michigan, Ann Arbor, Michigan, USA. Fax: 734-936-2778; Tel: 734-764-7541

[b]School of Public Health, University of Michigan, Ann Arbor, Michigan, USA

Abstract

Surface engineering of a hydrogel nanoparticle (NP) with the tumor-targeting ligand, F3 peptide, enhances both the NP's binding affinity for, and internalization by, nucleolin overexpressing tumor cells. Remarkably, the F3-functionalized NPs consistently exhibited significantly lower trafficking to the degradative lysosomes than the non-functionalized NPs, in the tumor cells, after internalization. This is attributed to the non-functionalized NPs, but not the F3-functionalized NPs, being co-internalized with Lysosome-associated Membrane Protein-1 (LAMP1) from the surface of the tumor cells. Furthermore, it is shown that the intracellular trafficking of the F3-functionalized NPs differs significantly from that of the single F3 peptides. This has important implications for designing effective, chemically-responsive, controlled-release and multifunctional nanodrugs for multi-drug-resistant cancers.

Introduction

Targeted multifunctional nanocarriers are generally nanoparticles with integrated, multivalent tumor-targeting moieties, diagnostic-imaging agents and therapeutic components, which, in combination, facilitate *in vivo* theranostics, with the aim of overcoming the specificity and efficacy limitations of conventional cancer diagnostic and therapeutic approaches.[1,2] Successful integration of these chemically diverse entities within a single nanoparticle, while retaining their respective biochemical/biophysical properties, requires a highly versatile, yet stable and biocompatible matrix. The first described multifunctional, multivalent nanocarriers were based on the synthetic polymeric hydrogel matrix, polyacrylamide (PAA), which easily facilitates multifunctionality due to its chemical flexibility.[3–7] In the last decade, both natural and synthetic polymeric hydrogels have emerged as promising nanoplatforms for the development of biocompatible targeted multifunctional nanocarriers.[8] This is enabled by the special properties of hydrogels, *namely,* hydrophilicity,[9] low cytotoxicity,[10] biodegradability,[11–14] capacity for high-density co-encapsulation of multiple payload types, including a broad range of drugs,[15] contrast agents for biomedical imaging,[3–8,16–18] biosensing probes, [19–21] and photosensitizer chemicals for photodynamic therapy,[4–8,22–24] while simultaneously protecting their

†Electronic Supplementary Information (ESI) available: Effect of Potassium depletion on F3 peptide subcellular localization, MTT cytotoxicity data for endocytic inhibitors, size and morphology characterizations of hydrogel PAA nanocarriers, and optimization data for nanocarrier surface functionalization with PEG molecules and F3 peptides. See DOI: 10.1039/b000000x/

Correspondence to: Raoul Kopelman, kopelman@umich.edu.

‡L. Karamchand and G. Kim are equally contributing first authors.

payloads against chemical/enzymatic degradation.[25] Another attractive feature of polymeric hydrogel nanocarriers is their engineerability for controlled release in response to a broad range of stimuli,[26] which permits their 'tuning' to the physiological environment of tumors, for optimal drug release. A question underlying this work is whether nano-drugs with their multiple targeting ligands can overcome cellular multi-drug resistance (MDR) faced by single molecule drugs using the very same targeting ligands.

Optimal drug release from chemically-responsive, controlled-release hydrogel nanocarriers, in particular, which are engineered to liberate their therapeutic payloads in response to a specific intracellular stimulus, such as pH,[27] glutathione[28,29] or lysosomal enzymes,[30] is predicated on their 'directive targeting' to the appropriate subcellular compartment. This is dependent on the endocytic pathway via which the target cell initially internalizes the hydrogel nanocarrier, and in turn, has direct bearing on the efficacy of the drug in its target tumor cell. In non-phagocytic cells, the major endocytic pathways that mediate the internalization of nanocarriers include the clathrin-mediated, caveolae-mediated and macropinocytosis pathways.[31] Nanocarriers that are internalized via either the clathrin-mediated or macropinocytosis pathways ultimately accumulate within lysosomes (degradative, acidic vesicles), whereas those internalized via caveolae-mediated endocytosis typically accumulate within non-degradative vesicles of neutral pH, known as caveosomes. Recent studies have demonstrated that the internalization and intracellular trafficking of a hydrogel nanocarrier is influenced by its ensemble of unique physicochemical properties, namely; size,[32–34] morphology,[35,36] elasticity of the hydrogel matrix,[37] and surface charge.[38–40] In addition to these physicochemical parameters, the surface engineering of a hydrogel nanocarrier with targeting ligands that bind selectively to specific receptors, which are overexpressed exclusively on the cell membrane of tumor and/or tumor endothelial cells, also influences the internalization and, subsequently, the intracellular trafficking of the nanocarrier. This strategy of nanocarrier 'molecular addressing' serves to enhance the nanocarrier's binding affinity for, and internalization by, the target tumor/endothelial cell, while relying on the assumption that the ligand-bearing nanocarrier will be internalized and trafficked along the same endocytic pathway as the ligand alone.

Targeting of drug-laden nanocarriers to cell surface receptors that are overexpressed on the surface of tumor and/or tumor endothelial cells, with the specific capacity of translocation into the nucleus, is especially crucial to the efficacy of chemotherapeutic drugs whose site of action is in the nucleus. Nucleolin, a nucleolar phosphoprotein that possesses a bipartite nuclear localization signal (NLS),[41] is such a receptor that is overexpressed on the surface of tumor endothelial cells, as well as on some other types of tumor cells.[42] Nucleolin has already been exploited for the targeted *in vivo* delivery of multifunctional PAA hydrogel nanocarriers to tumors in which it is overexpressed.[7,43] This has been achieved using the F3 peptide, a 32 amino acid sequence (KDEPQRRSARLSAKPAPPKPEPKPKKAPAKKC),[44] as the nucleolin-targeting ligand. However, an important consideration in the NLS receptor-mediated transport of nanocarriers/nanoparticles into the nucleus is the size-restriction imposed by the nuclear pore complexes (~40 nm) on the entry into the nucleus of cargo that exceeds this size-restriction,[45] as well as the intracellular fate of such ligand-targeted nanocarriers/nanoparticles. Recent studies in our lab on nucleolin-overexpressing cell lines, involving two-photon microscopy analysis of F3-targeted and non-targeted, pH-sensing PAA nanocarriers (68 nm) and silver core/PAA shell nanocarriers (90 nm and 130 nm), revealed that, although the F3-targeted PAA nanocarriers were not transported into the nuclei, they were instead sequestered within membrane-bound vesicles, but did not accumulate within lysosomes, whereas non-targeted PAA nanocarriers accumulated within lysosomes.[46,47] This observation led us to pose the question, which forms the basis of this present study: *How transferable is the intracellular targeting property of the F3 peptide to a hydrogel nanocarrier surface functionalized with this ligand?* Remarkably, we observed that

while the inhibition of clathrin-mediated endocytosis promoted the internalization of the single, monovalent F3 peptide and its translocation into the nucleus, the inhibition of this pathway instead strongly inhibited the internalization of the F3-targeted PAA nanocarriers. Furthermore, in the absence of inhibitors of the clathrin endocytic pathway, the former normally accumulates within lysosomes without translocation to the nuclei, whereas the latter accumulates within endosome-type vesicles, *but evades trafficking to the lysosomes*. This novel finding suggests that the coupling of multiple F3 peptides to the surface of the PAA nanocarrier, i.e. its multivalency, significantly alters the intracellular trafficking property of the peptide, and underscores the importance of not assuming that a ligand-bearing nanocarrier will follow the same intracellular trafficking pathway as that of the ligand alone. To the best of our knowledge, this study constitutes the first attempt at *elucidating the influence exerted by the F3 peptide surface functionalization of a nanocarrier/nanoparticle on both its internalization and intracellular trafficking in tumor cells*. Furthermore, we believe that the approach presented here will also be applicable to elucidate the endocytosis and intracellular trafficking pathways employed by nanocarriers functionalized with other targeting moieties, aimed at other cell surface-expressed proteins, with the goal of overcoming the multidrug resistance of cancer cells. We present here the overall result in schematic form (as suggested by a reviewer), so as to assist the reader with following the details of the study that lead to this conclusion (see Scheme 1).

Results and Discussion

Endocytic Inhibition of Nanocarrier Internalization in Nucleolin-overexpressing cell lines

Different endocytic pathways, particularly clathrin-mediated and caveolae-mediated endocytosis and macropinocytosis, have been implicated in the cellular internalization of nanocarriers, depending on the physicochemical properties of the nanocarrier.[31] Given the influence of a hydrogel nanocarrier's physicochemical properties on its cellular internalization, we employed an F3-targeted PAA hydrogel nanocarrier (F3NC), which is similar to that of an unmodified, *non-targeted* PAA hydrogel nanocarrier (NTNC) in terms of physicochemical properties, i.e. size and surface charge (see Supplementary Figs. S3–S5). We employed the inhibitors, chlorpromazine (CPZ), genistein (GEN) and cytochalasin D (CD), which specifically disrupt the above-mentioned endocytic pathways, respectively, and compared the behavior of the multivalent FITC-labeled F3NCs, under the same conditions, with that of the FITC-labeled NTNCs and FITC-labeled monovalent, molecular F3 peptides (molecular-F3 peptides), in separate cultures of live 9L and MDA-MB-435 cells. These cells are known to overexpress nucleolin receptors at their surfaces. The additional labeling of the lysosomes with a pH-sensitive fluorophore, Lysotracker Red DND-99, permitted simultaneous assessment of whether the fluorescent F3NCs, NTNCs and molecular-F3 peptides accumulate within lysosomes, in the absence or presence of any of the endocytosis inhibitors. All confocal images were analyzed according to three criteria, namely, (i) the degree of cellular uptake, (ii) the degree of colocalization with Lysotracker Red and, (iii) the absence or presence of nuclear accumulation of molecular-F3 peptides/ NTNCs/ F3NCs.

Interestingly, neither of the inhibitors completely blocked the endocytosis of molecular-F3 peptide, in both 9L and MDA-MB-435 cell lines. While both CD and GEN elicited comparably low levels of inhibition (~20–30%) on the internalization of molecular-F3 peptide, CPZ instead enhanced the internalization of molecular-F3 peptide in both cell lines, relative to the untreated controls (Figs. 3.1 and 3.2). Furthermore, CPZ promoted prominent accumulation of molecular-F3 peptide in the nuclei of both 9L (Fig. 1.1.c) and MDA-MB-435 (Fig. 2.1.c) cells, with the accumulation of molecular-F3 peptide being highest in the nucleolar regions of the nuclei. Potassium depletion, a potent non-pharmacological inhibitor of clathrin-mediated endocytosis, also promoted prominent nuclear accumulation of molecular-F3 peptide, in both the 9L and MDA-MB-435 cells (see Supplementary Fig.

S1). However, molecular-F3 peptide was not observed in the nuclei of the control, CD- or GEN-treated 9L (Figs. 1.1.a, b, d) and MDA-MB-435 cells (Figs. 2.1.a, b, d). Colocalization (yellow/orange fluorescent punctate foci) between molecular-F3 peptide (green) and Lysotracker Red was observed in the control (no inhibitors), CD- and GEN-treated 9L (Figs. 1.1.a, b, d) and MDA-MB-435 (Figs. 2.1.a, b, d) cells, although the degree of colocalization in MDA-MB-435 cells (~90%, Fig. 4.2) was markedly greater than that in 9L cells (~35%, Fig. 4.1). However, in both CPZ-treated 9L and MDA-MB-435 cells (Figs. 1.1.c and 2.1.c), the degree of colocalization between molecular-F3 peptide and Lysotracker Red was markedly lower (7.2 % and 3.5 % respectively) than in the control, CD- and GEN-treated cells (Figs. 4.1. and 4.2.).

In contrast to the observations for the molecular-F3 peptide, both CPZ and GEN elicited marked reductions in the internalization of the NTNCs in both cell lines; 38.1% and 55.5% internalization respectively for 9L cells (Fig. 3.1), and 42.1% and 52.8% internalization respectively for MDA-MB-435 cells (Fig. 3.2). The greater inhibitory effect of CPZ on the internalization of the NTNCs is evident from the NTNCs being confined mostly to the cell peripheries (Figs. 1.2.c and 2.2.c). In both cell lines, CD exerted a lower inhibitory effect on the internalization of the NTNCs, which was similar to the level of inhibition exerted on the internalization of molecular-F3 peptide in the respective cell lines (Figs. 3.1 and 3.2). Importantly, over the duration of the experiment (2–3 hours), the NTNCs did not enter the nuclei of the controls (Figs. 1.2.a and 2.2.a) or any of the endocytosis-inhibitor treatments, in either of the cell lines (Figs. 1.2.b–d and 2.2.b–d). The degree of colocalization between the NTNCs and Lysotracker Red was 2-fold higher in the MDA-MB-435 control cells (46.5%) than in the 9L control cells (22.1%) (Figs. 4.1 and 4.2). All endocytic inhibitors decreased the degree of colocalization between the NTNCs and Lysotracker Red, relative to the control, in MDA-MB-435 cells, whereas only CD and CPZ decreased the degree of colocalization between the NTNCs with Lysotracker Red, relative to the control, in 9L cells. Nonetheless, the degree of NTNC-Lysotracker Red colocalization in CD- and GEN-treated MDA-MB-435 cells remained higher than the corresponding inhibitor treatments in the 9L cells. Notably, CPZ was the most potent inhibitor in reducing the colocalization between the NTNCs and Lyostracker Red in both cell lines; 7.1% and 7.2% colocalization for the 9L and MDA-MB-435 cells, respectively (Figs. 4.1 and 4.2).

As observed for the NTNCs, F3NC internalization was most potently inhibited by CPZ in both the 9L (23.3%; Figs. 1.3.c and 3.1) and MDA-MB-435 cells (37.7%; Figs. 2.3.c and 3.2). Notably, F3NC internalization in both CPZ-treated cell lines were lower than, although not significantly different from, NTNC internalization in the CPZ-treated 9L (38.1%) and MDA-MB-435 (42.1%) cells. In contrast, F3NC internalization in the GEN-treated 9L (65.7%) and MDA-MB-435 (78.9%) cells were higher than NTNC internalization in the GEN-treated 9L (55.5%) and MDA-MB-435 (52.8%) cells (Figs. 3.1 and 3.2). Interestingly, F3NC internalization was lower in CD-treated MDA-MB-435 cells (63.1%) than CD-treated 9L cells (81.2%), although these levels of F3NC internalization were not significantly different from NTNC internalization in CD-treated 9L (77.8%) and MDA-MB-435 (67.4%) cells (Figs. 3.1 and 3.2). Most importantly, there was no observable permeation of the F3NCs into the nuclei of the controls (Figs. 1.3.a and 2.3.a), or for any of the endocytic inhibitor treatments (Figs. 1.3.b–d and 2.3.b–d), in either cell line. The absence of nuclear entry by the F3NCs, particularly in the presence of CPZ, is especially interesting in light of the nuclear accumulation of molecular-F3 peptide when mediated by CPZ (Figs. 1.1.c and 2.1.c). Most strikingly, the degree of colocalization of the F3NCs with Lysotracker Red was significantly lower than for molecular-F3 peptide and NTNCs in the control, CD- and GEN-treated 9L and MDA-MB-435 cells (Figs. 4.1 and 4.2). For example, in the 9L control cells, F3NC-Lysotracker Red colocalization was 3-fold and 1.8-fold lower than for molecular-F3 peptide and the NTNCs, respectively, while in the MDA-MB-435 control cells, F3NC-

Lysotracker Red colocalization was 6.4-fold and 3.3-fold lower than for molecular-F3 peptide and the NTNCs, respectively. As observed for molecular-F3 peptide and the NTNCs, the degree of F3NC-Lysotracker Red colocalization was most potently reduced by CPZ in both 9L (6.0%) and MDA-MB-435 (4.7%) cells, relative to the untreated control 9L (12.5%) and MDA-MB-435 (14.2%) cells (Figs. 4.1 and 4.2). These levels of colocalization were also similar to those observed for molecular-F3 peptide and the NTNCs in the CPZ-treated 9L and MDA-MB-435 cells (Figs. 4.1 and 4.2).

The observations from the endocytosis inhibition experiments indicate that: (i) neither macropinocytosis, clathrin-mediated, nor caveolae-mediated endocytosis are utilized by the molecular-F3 peptide as its primary pathway of cellular entry into either 9L or MDA-MB-435 cells; (ii) the above endocytic pathways each promote, to varying degrees, the internalization of the NTNCs and F3NCs, of which clathrin-mediated endocytosis is the major internalization pathway; and (iii) the F3NCs are more efficient than both the molecular-F3 peptide and the NTNCs at evading trafficking to the lysosomes and thus accumulate within different ‘endosomal-type’ vesicles, with this disparity being most prominent in the MDA-MB-435 cell line. Given the observation that a greater fraction of the endocytosed NTNCs, compared to the F3NCs, accumulate within lysosomes in MDA-MB-435 cells, we subsequently probed the intracellular trafficking of these two types of nanocarriers, independently of each other, in MDA-MB-435 cells, by immunocytochemistry, to gain further insight into the mechanism behind the selective accumulation of the targeted and non-targeted nanocarriers within different subcellular vesicles.

Spatiotemporal Probing of Nanocarrier Intracellular Trafficking by Immunocytochemistry

Separate batches of MDA-MB-435 cells, treated with either NTNCs or F3NCs, were fixed at various time points up to 6 hours after delivery of the NCs, following which, the cells were labeled for lysosome associated membrane protein 1 (LAMP1) and either early endosome antigen 1 (EEA1), which is associated with clathrin-mediated pathway, or caveolin 1 (caveolae marker), and analyzed by confocal microscopy. The rationale behind this approach was to obtain snapshots of any potential interaction between the FITC-labeled NTNCs/F3NCs and the above-mentioned markers from internalization, and throughout their intracellular trafficking within the MDA-MB-435 cells. Therefore, the absence or presence of colocalization between the NTNCs/F3NCs and these markers facilitated further examination of the endocytic pathway(s) responsible for internalizing each of these NCs and, more importantly, if the F3NCs are indeed able to evade trafficking to the lysosomes. All confocal images were analyzed on the basis of (i) the degree of colocalization between the NTNCs/F3NCs with EEA1, Caveolin1 or LAMP1 and, (ii) the absence or presence of nuclear accumulation of the NTNCs/F3NCs. Distinct differences were observed between the F3NCs and NTNCs with respect to their interaction with, and intracellular trafficking within, the MDA-MB-435 cells.

The most prominent feature of the F3NC-treated MDA-MB-435 cells is the distinct delineation of their cell membranes with the green-fluorescent F3NCs. These cell membrane delineations were evident at all time points, up to 180 min post-delivery (Figs. 5.2.a–e & 6.2.a–e); however by 360 min post-delivery, the cell membrane delineations had markedly diminished, concomitant with prominent endosomal accumulation of the F3NCs (Figs. 5.2.f and 6.2.f). This observation suggests that, by 360 min post-delivery, the majority of the cell-membrane-bound F3NCs were endocytosed by the MDA-MB-435 cells. Interestingly, despite the high avidity of the F3NCs for the nucleolin over-expressing MDA-MB-435 cells, the appearance of F3NC-laden endosomes within the cytoplasm was most evident only at 30 minutes (Figs. 5.2.b and 6.2.b) and onward of delivery (Figs. 5.2.c–f, 6.2.c–f).

At 10 minutes after delivery, only 7.8% of the F3NCs colocalized with EEA1 (Figs. 5.2.a, 7.1), which then peaked to 32.7% colocalization at 30 minutes post-delivery (Fig. 5.2.b, 7.1), and thereafter decreased progressively to 3.9% colocalization by 360 minutes post-delivery (Figs. 5.2.c–f, 7.1). Colocalization between the F3NCs and Caveolin1 was diffuse and confined exclusively to the cell surface; unlike the distinct punctate foci of colocalization observed between the F3NC-laden endosomes and EEA1 within the cytoplasm. At 10 minutes after delivery, 6.9% of the cell membrane-bound F3NCs colocalized with Caveolin1 (Fig. 6.2.a), which then peaked to 14.5% colocalization at 120 minutes post-delivery (Fig. 6.2.d), and thereafter decreased progressively to 6.2% by 360 minutes post-delivery (Figs. 6.2.e, f, 7.2). Furthermore, only scant colocalization between the F3NCs and LAMP1 was observed at the various time points (Figs. 5.2.a–f and 6.2.a–f; dashed white arrows). At 10 minutes after delivery, only 7.9% of the F3NCs colocalized with LAMP1, which then peaked to 8.2% colocalization at 30 minutes post-delivery, and thereafter decreased progressively to 4.7% colocalization by 360 minutes post-delivery (Fig. 7.3). Most notably, from 60 minutes after delivery and onward, larger F3NC-laden endosomes that exhibited an absence of colocalization with the EEA1, Caveolin1 and LAMP1 markers, began to accumulate, which suggests that the F3NCs are sequentially trafficked from the early endosomes to late endosomal vesicles (Figs. 5.2.c–f and 6.2.c–f), since the late endosomes are devoid of EEA1 and Caveolin1 markers. Moreover, some of these ‘larger’ F3NC-laden endosomes appeared within the perinuclear region from as early as 120 minutes after delivery and onward (Figs. 5.2.e, f and 6.2.d–f), although there was no observable entry or accumulation of F3NCs within the nuclei of the cells (Figs. 5.2.d–f and 6.2.d–f).

In stark contrast to the F3NC-treated cells processed for immunocytochemistry, cell membrane delineations were not observed with the NTNCs at any of the time points investigated (Figs. 5.1.a–f and 6.1.a–f). Given the inherent non-specific affinity of the NTNCs for negatively charged cell membranes, due to their modest positive surface charge (~ +16 mV, Supplementary Fig. S4), in addition to the appearance of NTNC-laden endosomes in the periphery of the cytoplasm just 10 minutes after delivery (Figs. 5.1.a and 6.1.a), these observations suggest that the NTNCs are endocytosed slightly faster than the F3NCs upon contact with the cell membrane. In contrast to the F3NCs, a greater fraction of the NTNC-laden endosomes (23.4%; Fig. 7.1) were colocalized with EEA1 at 10 minutes after delivery (Figs. 5.1.a, solid white arrows), which correlated with the faster appearance of NTNC-laden endosomes in the cytoplasm at this time point. As observed for the F3NCs, the degree of colocalization between the NTNC-laden endosomes and EEA1 peaked to 32.6% colocalization at 30 minutes post-delivery (Fig. 5.1.b), and thereafter decreased progressively, but still remained as high as 14.8% by 360 minutes post-delivery (solid white arrows; Figs. 5.1.c–f, 7.1). Distinct punctate colocalization was observed between the NTNCs and Caveolin1 – positive endosomes both at the cell surface and within the cytoplasm (Figs. 6.1.d–f; solid white arrows). This contrasts with the colocalization between the F3NCs and Caveolin1, which was scant and confined exclusively to the cell surface (Figs. 6.2.a–f; solid white arrows). At 10 minutes after delivery, 6.6% of the NTNCs colocalized with Caveolin1 (Fig. 6.1.a), which then peaked to 28.5% colocalization at 120 minutes post-delivery (Fig. 6.1.d), and thereafter decreased to 8.6% colocalization by 360 minutes post-delivery (Figs. 6.1.e, f, 7.2). In stark contrast to the F3NC-treated cells, the NTNCs colocalized strongly with LAMP1, appearing as distinct punctate foci of orange/yellow fluorescence (dashed white arrows), both at the cell surface and in NTNC-laden endosomes within the cytoplasm (Figs. 5.1.a–f and 6.1.a–f). At 10 minutes after delivery, 20.3% of the NTNCs colocalized with LAMP1 (compared to 7.9% F3NC-LAMP1 colocalization at 10 minutes), which increased sharply to 44.9% colocalization at 60 minutes post-delivery, and peaked to 49.2% colocalization at 180 minutes post-delivery (Fig. 7.3). A slight decrease to 45.3% colocalization was observed at 360 minutes post-delivery, however

this was not significantly different from the degree of colocalization at 180 minutes post-delivery (Fig. 7.3). Therefore, the degree of colocalization between the NTNCs and LAMP1 increased with time and was significantly higher than that for the F3NCs at each time point, whereas the colocalization between the F3NCs and LAMP1 decreased with time. Moreover, NTNC-laden endosomes that exhibited dual-colocalization with LAMP1 and either EEA1 or Caveolin1 were also observed (Figs. 5.1.a, c–f and 6.1.e, f; white triangles). Importantly, as observed for the F3NCs, the NTNC-laden endosomes did not enter the nuclei, and largely remained dispersed throughout the cytoplasm.

Cell Membrane Interaction Profiles of Non-targeted and F3-targeted PAA-NCs

Our immunocytochemical analyses revealed a fundamental difference between the F3NCs and NTNCs, with respect to their interactions with the cell membranes of MDA-MB-435 cells in that, the F3NCs elicited prominent delineation of the MDA-MB-435 cell membranes, whereas this effect was not observed with the NTNCs. Cell membrane delineations were however observed for the NTNC-treated cells in the endocytosis inhibition images, but were less prominent than that observed for the F3NC-treated cells. Interestingly, prominent appearance of the F3NC-laden endosomes in the cytoplasm occurred only 30 minutes after delivery, whereas NTNC-laden endosomes appeared in the cytoplasm as early as 10 minutes after delivery. These observations indicate that the F3NCs first accumulate on the cell membrane, upon binding, for a significant period of time before being internalized, whereas the NTNCs do not accumulate on the cell membrane and are internalized fairly rapidly upon contact with the cell membrane. *Thus, there must be a difference between the F3NCs and NTNCs in their interaction with the MDA-MB-435 cell membrane.* Notably, the binding of positively charged nanoparticles to negatively charged cell membranes is driven by non-specific electrostatic interactions. Furthermore, it has been demonstrated that the binding of amine-surface modified polystyrene nanoparticles to dipalmitoyl phosphocholine (DPPC) liposomes induces a lipid phase transition, from gel to fluid, at the nanoparticle-membrane interface,[48] which may potentiate the detachment of invaginating endosomes that form around the nanoparticle from the cell membrane.[49] Hence, our positively charged, amine-surface modified NTNCs may elicit a similar lipid phase transition in the regions of the MDA-MB435 cell membranes to which they bind, thereby potentiating their rate of endocytic uptake.

In contrast, while the F3NCs have a higher positive surface charge (~ +30 mV) than the NTNCs (~ +16 mV) (see supplementary information; Figs. S4 and S5), the interaction of the former with the MDA-MB-435 cell membrane is limited to the binding interaction between their surface-conjugated F3 peptides and the cell surface bound nucleolin receptors. Furthermore, targeted nanoparticles of 50 nm in diameter and greater bind numerous receptors simultaneously with very high avidity (~$1–3 \times 10^{-13}$ M),[50] such that the internalization of further nanoparticles is limited by the redistribution of additional receptors on the cell membrane by lateral diffusion in order to compensate for the depletion of unbound cell surface receptors in the contact region between the cell membrane and nanoparticle.[51] The uptake of additional nanoparticles may be further limited by the rate at which new receptors are delivered to the cell membrane,[52] in order to compensate for those receptors that have been internalized along with the bound nanoparticle, as is the case with nucleolin.[53] This phenomenon provides a plausible explanation for the slightly longer lag time observed between the delivery of the F3NCs and their first appearance in the cytoplasm, compared to the NTNCs. This is attributed to the properties of the F3NCs, i.e. their hydrodynamic size of ~60 nm and their ligand surface coverage that elicits cell binding saturation (see supporting information, Figs. S3.3 and S6), and is in accordance with previous observations.[50,51]

Evidence in support of the specificity of the interaction between the F3-surface functionalized PAA-NCs and the nucleolin receptors is provided by a control experiment that was performed in a recent study published by our lab,[54] whereby we functionalized PAA-NCs with either the wild-type F3 peptide or a scrambled F3 peptide (identical amino acid composition, length and charge, but scrambled sequence) and compared the uptake of these functionalized nanocarriers in the nucleolin surface-expressing 9L cell line. The wild-type F3 peptide promoted uptake of the PAA-NCs, whereas the scrambled F3 peptide did not. This observation indicates that only the wild-type F3 peptide sequence is capable of adopting the correct secondary and/or tertiary conformation that is necessary for binding to the cell-surface nucleolin receptors, and thus promoting uptake of the nanocarriers.

Internalization and Intracellular Trafficking Profiles of F3 peptide, F3-targeted and Non-targeted PAA-NCs

After internalization, the drug-laden nanocarrier should ideally be delivered to the specific subcellular compartment within which that drug molecule elicits its mechanism of action, in order to circumvent extrusion of these drug molecules by the cell membrane-resident multidrug resistance (MDR) efflux pumps, *and thereby retain the efficacy of therapy*. Although recent studies have demonstrated that the physicochemical properties of a nanocarrier modulates its intracellular trafficking,[55,56] it still remained unclear, prior to our current study, as to how the presence of multiple copies of a targeting ligand on the surface of a nanocarrier, i.e. its multivalency, influences its intracellular trafficking and subcellular accumulation, relative to its non-targeted counterpart, or even relative to the targeting ligand alone. An important observation from our endocytosis inhibition study is that neither of the endocytic inhibitors, CD, CPZ or GEN, completely blocked the internalization of the NTNCs or F3NCs, but each one decreased the internalization of the various nanocarriers to varying degrees. Since only one endocytic inhibitor was used at a time, so as to minimize cytotoxicity, the other endocytic pathways would have been still operational, and thus able to promote the uptake of the nanocarriers. This would account for why we did not observe complete inhibition of the uptake of the NTNCs and F3NCs in the presence of any one inhibitor.

Our endocytosis inhibition data demonstrated that (i) the intracellular trafficking of molecular-F3 peptide in its monovalent form is markedly different compared to when it is coupled to the surface of hydrogel PAA-NCs and (ii), although the non-targeted and F3-targeted PAA-NCs share common pathways of internalization, albeit to varying degrees, they each accumulate in distinct types of subcellular vesicles. We acknowledge that although the F3 peptides used in our experimental setup were not in their ‘native form’ i.e. they were chemically labeled with FITC fluorophore, the significantly smaller size of the FITC fluorophore (389 Da), compared to that of a single F3 peptide (3536 Da) or a single PAA-NC, has negligible, if any, effect on the behavior of the F3 peptide. Furthermore, the FITC fluorophore has only one reactive isothiocyanate group, and is therefore incapable of cross-linking multiple F3 peptides, so as to generate a multivalent peptide complex, which would likely alter the binding avidity of the F3 peptide for Nucleolin as well as alter its intracellular trafficking. The intracellular trafficking of monovalent molecular-F3 peptide is particularly interesting in that it inherently accumulated in lysosomes, with neither of the endocytic inhibitors CD or GEN being able to completely prohibit its cellular entry or accumulation in lysosomes. While CPZ also failed to prohibit the cellular entry of molecular-F3 peptide, it however *promoted a diversion in the trafficking of the molecular-F3 peptide from the lysosomes to the nucleus*. We observed the same result for molecular-F3 peptide in both the 9L and MDA-MB-435 cell lines when the cells were subjected to potassium depletion (Supplementary Fig. S1), which acts as a potent non-pharmacological inhibitor of the clathrin-mediated endocytic pathway. This phenomenon is therefore not

unique to chlorpromazine, and we conclude that the inhibition of the clathrin-mediated pathway, irrespective of the inhibitor, promotes accumulation of molecular-F3 peptide within the nuclei of 9L and MDA-MB-435 cells. Notably, our observations are consistent with the study by Legrand *et al.*, which first documented that the cellular uptake of the human Lactoferrin protein (hLf) is mediated by nucleolin and that the majority of these nucleolin-hLf complexes colocalize with EEA1, a marker specifically associated with clathrin in early endosomes.[57] Our findings therefore confirm that the cell's surface-bound nucleolin is associated with the clathrin-mediated endocytic pathway, which likely overrides the nuclear localization signal (NLS) of nucleolin and thus promotes the routing of the molecular-F3 peptide into the lysosomes. However, upon inhibiting the clathrin-mediated endocytic pathway by CPZ, the NLS function of nucleolin apparently predominates, thereby allowing translocation of nucleolin, together with any bound molecular-F3 peptide, directly into the nucleus. Given our observations with molecular-F3 peptide, we might have anticipated a similar intracellular trafficking pattern for the F3NCs, however this was not the case. Remarkably, in the absence, as well as the presence, of endocytic inhibitors, the F3NCs exhibited markedly lower accumulation within lysosomes as compared to molecular-F3 peptide and to the NTNCs, in both 9L and MDA-MB-435 cells. Most notably, CPZ was the only inhibitor that elicited a marked reduction in both the endocytosis and lysosomal accumulation of the F3NCs, in either cell line. A similar result was observed for the NTNCs in both the CPZ-treated 9L and MDA-MB-435 cells. Therefore, these data suggest that while the F3NCs and the NTNCs share clathrin-mediated endocytosis as a common pathway of internalization, *the multivalent nature of the F3-targeted PAA nanocarrier significantly alters its intracellular trafficking within these cell lines, so as to avoid accumulation within the lysosomes.* It should be noted that while not all endocytosed NTNCs were found to colocalize with Lysotracker Red at 1 hour after delivery, it is likely that these NTNCs were sequestered within early and/or late endosomes that were still *en route* for fusion with lysosomes. Evidence in support of this premise is provided by our immunocytochemistry data in which only the NTNCs exhibited a time-dependent increase in colocalization with lysosome associated membrane protein 1 (LAMP1), over the 6-hour period during which the intracellular trafficking of the NTNCs was observed (Fig. 7.3).

The immunocytochemical analysis also corroborated the findings of the endocytosis inhibition experiment in MDA-MB-435 cells that clathrin-mediated endocytosis contributed approximately equally to the internalization of the NTNCs and F3NCs, while the caveolae-mediated pathway mediated greater internalization of the NTNCs than the F3NCs. This is evident from the observations that (i) CPZ decreased the internalization of the NTNCs and F3NCs to similar levels (Fig. 3.2), while the colocalization of the NTNCs and F3NCs with EEA1 both peaked at 30 minutes post-delivery to similar levels (Fig. 7.1), and (ii) in GEN-treated cells, the level of NTNC internalization was approximately 1.49-fold lower than that of the F3NCs (Fig. 3.2), while the peak NTNC-Caveolin1 colocalization at 120 min post-delivery was approximately 1.96-fold higher than that of the F3NC-CAV1 colocalization at the same time point (Fig. 7.2). These observations suggest that the presence of multiple F3 peptides on the surface of the F3NCs biases their internalization via the clathrin-mediated endocytic pathway, as compared to the NTNCs. From 60 min post-delivery, a progressive decrease in the colocalization with EEA1, for both the F3NCs and NTNCs, was observed, suggesting that both types of nanocarriers were being transported into the *late endosomes*, which lack the EEA1 marker. Interestingly, for both the F3NCs and NTNCs, the peak in colocalization with Caveolin1 was achieved only at 120 minutes post-delivery. This observation may be due to the existence of bidirectional communication between the clathrin-mediated and caveolae-mediated endocytic pathways, whereby cargo that is internalized via caveolae-mediated endocytosis can be trafficked into EEA1 – positive endosomal compartments, and vice versa.[58,59] It was also interesting to note that the macropinocytosis inhibitor, Cytochalasin D, exerted a slightly greater inhibitory effect than

Genistein on the internalization of the F3NCs in the MDA-MB-435 cells. This may be attributed to the previously reported observation that cell surface expressed Nucleolin is associated with the actin cytoskeleton,[60] and that Cytochalasin D inhibits macropinocytosis by disrupting actin polymerization.

F3-targeted PAA-NCs, but not Non-targeted PAA-NCs, evade co-internalization with LAMP1 at the cell surface

The most striking difference between the F3NCs and NTNCs in their intracellular trafficking is the presence of prominent punctate colocalization between the NTNCs and LAMP1, both at the cell surface and during their transport into the interior of the cells, at all time points, whereas such colocalization between the F3NCs and LAMP1 was scant over the 6-hour period during which their intracellular trafficking was tracked. This observation must be understood in the context of the trafficking of the newly synthesized lysosome-associated membrane proteins (LAMPs) themselves, and the role that these proteins play in the interaction between endosomes and lysosomes. First, the transport of newly synthesized LAMPs from the *trans*-Golgi network (TGN) to the lysosomes may follow either a direct or indirect pathway.[61,62] The direct pathway is a completely intracellular route whereby newly synthesized LAMPs are transported from the TGN to either early or late endosomes and then to lysosomes. In the indirect pathway, the LAMPs are first transported from the TGN to the extracellular surface of the cell membrane, subsequently internalized by the clathrin-mediated endocytic pathway,[63] and then sequentially delivered to the early endosomes, late endosomes and finally the lysosomes. Second, LAMPs are essential for facilitating fusion between phagosomes and lysosomes in macrophages,[64] and may very well be necessary for facilitating fusion between the late endosomes and lysosomes in other non-phagocytic cell types. It is therefore apparent from the positive cell surface labeling of the MDA-MB-435 cells with anti-LAMP1 antibody that (i) the indirect LAMP trafficking pathway is indeed operational in the MDA-MB-435 cell line, and (ii) the NTNCs, but not the F3NCs, are co-internalized with LAMP1 proteins from the cell surface via the clathrin-mediated pathway, which commits these NTNC-laden, EEA1-positive endosomes to undergo fusion with the lysosomes, as illustrated by their colocalization with Lysotracker Red in our live cell endocytosis inhibition experiment. Furthermore, the presence of NTNC-laden endosomes exhibiting dual-colocalization with LAMP1, and with either EEA1 or Caveolin1, indicates that, despite being trafficked via either the clathrin-mediated or caveolae-mediated endocytic pathways, the NTNC-laden endosomes are still committed to undergo fusion with the lysosomes. Moreover, the time-dependent increase in colocalization between the NTNCs and LAMP1 confirms that the NTNCs do accumulate within the lysosomes over time. Scheme 1 illustrates the internalization and intracellular trafficking profiles of molecular-F3 peptide, the F3NCs and NTNCs in nucleolin-overexpressing cells based on our observations.

Considering that LAMP1 is necessary for facilitating fusion between phagosomes and lysosomes, it is plausible that the absence of LAMP1 proteins in the F3NC-laden, EEA1-positive endosomes would abrogate the ability of these F3NC-laden late endosomes to fuse with lysosomes. The presence of large, punctate F3NC-laden, EEA1/LAMP1 – negative vesicles within the perinuclear space, 360 minutes after delivery, supports our postulate that the F3NCs accumulate within late endosomes, but without subsequent fusion with lysosomes. Given that the late endosomes can also fuse with the TGN, we speculate that the F3NCs may be transported into the nucleus via retrograde transport, through the endoplasmic reticulum, over longer periods of time. Exploiting this pathway would therefore serve as an alternative mechanism for delivering into the nucleus nanocarriers whose hydrodynamic diameters exceed the cut-off limit of the nuclear pore complexes, as is the case with our hydrogel polyacrylamide nanocarriers. Further studies are underway in our lab

to determine the long-term subcellular localization of the F3NCs in nucleolin-overexpressing cells.

Our observation that molecular-F3 peptide is normally trafficked to the lysosomes is consistent with a recent study which reported that nucleolin colocalizes with LAMP1 in the phagosomal compartment of macrophages.[65] Importantly, previous studies have also demonstrated that LAMP proteins are overexpressed at the surface of highly metastatic tumor cells.[66,67] The prominent cell surface labeling of the highly metastatic MDA-MB-435 cells[68] with anti-LAMP1 antibody in our study is therefore consistent with these studies. When taken into consideration with these previous reports, our observations suggest that the high surface density of LAMP1 proteins in the highly metastatic MDA-MB-435 cells increases the likelihood of nucleolin being co-internalized with LAMP1 proteins, which in turn commits the nucleolin-laden endosome to fusion with the lysosomes. Paradoxically, this is not the case when the F3NCs engage nucleolin receptors at the surface of MDA-MB-435 cells and are internalized. The reasons for this apparent paradox may be related to the following questions: (i) How exactly do the F3NCs evade co-internalization with LAMP1 proteins and (ii) what prohibits the direct translocation of newly synthesized LAMP1 proteins to those EEA1-positive early endosomes transporting the F3NCs, since our data indicate that clathrin-mediated endocytosis is a common pathway of internalization for both the F3NCs and the NTNCs?

Proposed mechanism for F3-targeted PAA-NC evasion of co- internalization with LAMP1

We believe that a plausible explanation of the above scenario lies in the nature of the binding interaction between P-selectin protein and the cell membrane-bound nucleolin receptors and the cell signal elicited as a result of this binding interaction. Reyes-Reyes and Akiyama recently identified nucleolin as the receptor for P-selectin protein in Colo-320 human colon carcinoma cells.[69] Furthermore, the authors demonstrated that the binding of P-selectin-IgG-Fc chimeric proteins to the surface of these cells induced clustering of nucleolin at the external surface of the cell membrane, followed by tyrosine phosphorylation of the clustered surface-resident nucleolin, specifically, which in turn led to the formation of a signalling protein complex comprising nucleolin, p38 mitogen activated protein kinase (MAPK) and phosphatidylinositol 3-kinase (PI3-K). *In vivo*, multiple P-selectin proteins would simultaneously engage multiple nucleolin receptors on the cell membrane of a malignant cell, thereby inducing nucleolin clustering, followed by formation of the nucleolin/p38 MAPK/PI3-K signalling complex, and subsequent endocytosis of this signalling complex.[70] W*e hypothesize* that this process of protein clustering, which promotes formation of the nucleolin/p38 MAPK/PI3-K signalling complex, physically excludes LAMP1 proteins from the region of the cell membrane undergoing invagination, in order to internalize this signalling complex. Similarly, since the F3NCs are multivalent entities of F3 peptide, it is conceivable that a single F3NC can simultaneously bind multiple nucleolin receptors. Therefore, the binding of F3NCs to the cell membrane of a nucleolin-overexpressing cell induces a clustering and phosphorylation of the nucleolin receptors at the extracellular surface of the cell membrane, promoting formation of the nucleolin/p38 MAPK/PI3-K signalling complex, which in turn excludes LAMP1 proteins from the membrane of the invaginating clathrin-endosome that mediates internalization of the bound F3NCs.

In addition to internalizing cargo from the extracellular environment, endosomes serve as fast communication highways, propelled by microtubular motors that play a crucial role in the rapid transport of signalling kinases (such as p38 MAPK and PI3-K), activated at the cell membrane, to the nucleus.[71,72] In light of the role that endosomes play in signal transduction, the exclusion of LAMP1 proteins from these ‘signalling endosomes’, which mediate internalization of the nucleolin/p38 MAPK/PI3-K complex, both during their

formation and during subsequent transit into the cell interior, would be essential to ensuring that these signalling kinases reach the nucleus, and not the lysosomes, where they would instead be degraded. Furthermore, it has already been demonstrated that the activation of p38 MAPK prohibits the fusion of phagosomes with lysosomes in murine macrophages; this being the mechanism by which *Mycobacterium tuberculosis* bacilli evade lysosomal degradation in macrophages.[73] It is possible that p38 MAPK similarly prohibits the fusion of signalling endosomes with LAMP1 – positive vesicles originating from the TGN and/or lysosomes in non-phagocytic cell types, such as MDA-MB-435 cells. Therefore, if the F3NCs do indeed induce the formation of, and are co-internalized with, the nucleolin/p38 MAPK/PI3-K signalling complexes, these F3NC-laden signalling endosomes may evade fusion with lysosomes, or LAMP1 – containing vesicles that originate from the TGN, by multiple mechanisms, as discussed.

Conclusions

Our investigation demonstrates that the presence of F3 peptide on the surface of the polyacrylamide hydrogel nanocarrier significantly modulates the nature of the nanocarrier's interaction with the cell membrane of the target cell, including not only its internalization but also its intracellular trafficking and subcellular localization, relative to the non-targeted nanocarrier. Furthermore, the ability of the F3-targeted hydrogel nanocarriers, but not of the molecular-F3 peptide, to evade trafficking to the lysosomes, strongly suggests that the *multivalent nature* of the F3-targeted hydrogel nanocarrier is responsible for this effect. The implications of our observations are two-fold. First, from a general perspective, it cautions against making the assumption that a targeted nanocarrier's fate within cells is solely determined by the targeting ligand, or solely the carrier, or by a combination of the respective properties of the ligand and carrier (which might adversely affect the efficacy of therapy). Second, and more specifically, our findings are particularly relevant to the targeting of highly metastatic tumor cells, and thus may provide new insights into a possible mechanism of preventing the co-internalization of drug nanocarriers with LAMP1, in order to circumvent their trafficking to lysosomes. This appears to have important implications regarding the potential advantages of nano-drugs with multivalent ligand targeting, compared to individual drug molecules containing an identical single targeting ligand, especially when it comes to overcoming the multi-drug resistance (MDR) of metastatic cancer cells. Also of much interest is the possibility of engineering nanoparticles that mimic natural pathogens' ability to overcome the cell's defence mechanisms. Further studies are being conducted in our lab to elucidate the mechanism by which the F3-targeted hydrogel nanocarriers circumvent trafficking to the lysosomes in nucleolin-overexpressing cell lines.

Experimental Section

Reagents and Materials

Acrylamide (AA), 3-(acryloyloxy)-2-hydroxypropylmethacrylate (AHM), ammonium persulfate (APS), *N,N,N′,N′*-tetramethylethylenediamine (TEMED), sodium dioctyl sulfosuccinate (AOT), Brij 30, L-cysteine, fluorescein isothiocyanate (FITC) and phosphate-buffered solution (PBS) tablets were purchased from Sigma-Aldrich (St. Louis, MO). N-(3-aminopropyl)-methacrylamide hydrochloride (APMA) was purchased from Polysciences (Warrington, PA). Ethanol (100 %) and hexane were purchased from Fisher Scientific (Pittsburgh, PA). Heterobifunctional polyethyleneglycol (MAL–PEG–SCM, MW: 2,000 Da) was purchased from Creative PEG Works (Winston Salem, NC). The 9L rat gliosarcoma and MDA-MB-435 human melanoma cell lines were obtained from American Type Culture Collection (Manassas, VA, USA). Dulbecco's modified Eagle medium (DMEM), Rosswell Park Memorial Institute (RPMI-1640) medium, Gibco 0.05 % Trypsin-EDTA, Gibco 100x PenStrep-Glutamine and Gibco Heat-Inactivated Fetal Bovine Serum (HI-FBS) were

purchased from Invitrogen (Carlsbad, CA). Endocytosis inhibitors, Cytochalasin D, Chlorpromazine, and Genistein were obtained from Sigma-Aldrich. Cysteine terminated F3 peptide (F3-Cys: KDEPQRRSARLSAKPAPPKPEPKPKKAPAKKC) was purchased from SynBioSci (Livermore, CA). Mouse monoclonal anti-EEA1, rabbit polyclonal anti-Caveolin1 and goat polyclonal anti-LAMP1 antibodies were purchased from Santa Cruz Biotechnology, Inc (Santa Cruz, CA, USA). Lysotracker Red DND-99, donkey anti-mouse (H+L) Alexa Fluor 568 (AF-568), donkey anti-rabbit (H+L) AF-568 and donkey anti-goat (H+L) Alexa Fluor 647 (AF-647) antibodies were obtained from Invitrogen. Normal donkey serum was purchased from LAMPIRE Biological Laboratories (Pipersville, PA). Methanol-free electron microscopy grade 20% (w/v) paraformaldehyde solution was purchased from Electron Microscopy Services (Hatfield, PA, USA). All solutions were prepared in 18 MΩ water purified in a Barnstead 1 Thermolyne Nanopure II system. All reagents and materials were used as received without further purification.

Synthesis of FITC-labeled amine surface-functionalized hydrogel polyacrylamide nanocarriers

A monomer mixture consisting of 1 mg FITC, 711 mg acrylamide, 55 mg APMA, and 460 μL AHM were dissolved in PBS buffer (pH 7.4) and mixed together for 2 hours at room temperature. The mixture was emulsified in organic media containing surfactant (45 mL hexane, 1.6 g AOT, and 3.1 g Brij30) by continuous stirring for 20 minutes under Argon atmosphere in order to purge the reaction mixture of oxygen. Thereafter, polymerization was triggered by addition of radical initiator (100 μL of 10 % (w/v) ammonium persulfate in DI water and 100 μL of TEMED). The reaction proceeded for 2 hours under mild argon purging and was terminated by exposing the reaction to normal atmosphere (radical quenching by atmospheric oxygen). The product was recovered through multiple separation steps: (i) removal of hexane by rotary evaporation, and (ii) multiple rinses with 100 % (v/v) ethanol to remove unconjugated FITC dye and surfactants, followed by multiple rinses with DI water to remove residual surfactants using an Amicon stirred cell fitted with a 300 kDa molecular weight cut-off filter. The final product was lyophilized and kept frozen at −20 °C until use.

Surface functionalizations of PAA nanocarriers

Lyophilized FITC-labeled PAA-NCs (50 mg) were dissolved in 2.5 mL PBS buffer (pH 7.4) and sonicated until the solution turned transparent, to which 4 mg heterobifunctional PEG (SCM-PEG-MAL) was then added and the mixture stirred continuously (~600 rpm) for 2 hours at room temperature. The reaction between the succinimidyl ester group of the PEG crosslinker and the primary amine groups on the surface of PAA-NCs yielded maleimidyl ester-terminated PEG-conjugated PAA-NCs. Thereafter, the PEGylated PAA-NCs were washed three times with DI water by centrifugation using an Amicon centrifugal filter (Millipore, 100 kDa molecular weight cut-off) at 5000*xg* for 20 min. The procedure was repeated twice more with PBS buffer (pH 7.4). After washing to remove unbound PEG crosslinkers, the surface PEGylated PAA-NCs were reacted with 11 mg F3-Cys peptide in PBS buffer (pH 7.4) and the conjugation reaction allowed to run overnight at room temperature under continuous stirring at ~600 rpm. The reaction between the thiol group of the carboxy terminal Cys residue of the F3 peptide moieties and the maleimidyl ester termini of the PEG crosslinkers facilitated covalent coupling of the F3 peptide moieties to the PEG crosslinkers already conjugated to the PAA-NC surfaces. The F3 surface functionalized PEGylated PAA-NCs (F3NCs) were subsequently incubated with 1.74 mg L-cysteine under continuous stirring for 2 hours at room temperature to cap any unreacted maleimidyl ester groups so as to prevent their reaction with cell surface thiols. Thereafter, the F3NCs were washed five times with PBS (pH 7.4) using an Amicon centrifugal filter (100 kDa molecular weight cut-off) at 4000x*g* for 20 minutes and the final volume adjusted to 5 mL with PBS

(pH 7.4). The filtered nanocarriers were kept frozen at −20 °C until use. All steps were performed shielded from light. Note that the mass ratios of heterobifunctional PEG and F3 peptide to PAA-NCs were optimized via cell-based assays as described in the supplementary information.

Synthesis of FITC-labeled F3 peptide

Stock solutions of F3-Cys peptide (100 $\mu g \cdot \mu L^{-1}$ in 10 mM phosphate buffer, pH 8.0) and FITC (160 $\mu g \cdot \mu L^{-1}$ in DMSO) were initially prepared. Thereafter, 10 μL of the FITC stock was added to 390 μL of F3-Cys solution in a clean glass vial and sonicated for 5 minutes. The final volume of the sonicated solution was increased to 10 mL with 10 mM phosphate buffer (pH 8.0), and the conjugation reaction was allowed to proceed overnight with continuous stirring at 37 °C while shielded from light. The following day, the FITC-labeled F3 peptides were subjected to 15 washes with a 3 kDa molecular weight cut-off Amicon centrifugal filter (4000*xg* for 20 minutes) to remove any unreacted FITC molecules. The filtered FITC-labeled F3 peptides were aliquoted and stored at −20 °C until further use.

Nanocarrier sizing and morphology

The size of the prepared F3NCs was determined via two different methods; scanning electron beam microscopy (SEM) and dynamic light scattering (DLS). Lyophilized F3NCs were dissolved in DI water to a final concentration of 0.2 $mg \cdot mL^{-1}$. A droplet of the NC solution was loaded onto a SEM stub, dried and subsequently coated with gold using a gold sputter coater. SEM imaging was performed using the FEI Nova NanoLab dualbeam SEM system. For all DLS sizing measurements, the lyophilized NCs were dissolved in DI water to a final concentration of 1 $mg \cdot mL^{-1}$ and analyzed with a Beckman-Coulter Delsa Nano C particle analyzer.

Nanocarrier zeta potential measurement

Zeta potential measurements of unmodified PAA-NCs (without PEG or F3 peptide), PEGylated PAA-NCs and the F3NCs were performed in order to determine their respective surface charges. All zeta potential measurements were performed on 1 $mg \cdot mL^{-1}$ solutions of each type of nanocarrier, prepared in DI water, using a Beckman-Coulter Delsa Nano C particle analyzer. All measurements were performed in triplicate.

Cell culture

Three different nucleolin-overexpressing tumor cell lines, 9L rat gliosarcoma, MDA-MB-435 human ductal adenocarcinoma/ melanoma, and MCF-7 human breast adenocarcinoma were cultured aseptically at 37 °C under 5 % CO_2 humidified atmosphere in either BD Falcon Primaria tissue culture dishes (100 mm × 20 mm) or Multiwell 6-well plates. The 9L and MCF-7 cell lines were cultured in Rosewell Park Memorial Institute (RPMI) medium supplemented with 10 % (v/v) heat inactivated fetal bovine serum (FBS) and MDA-MB-435 cell was cultured in Dulbecco's Modified Eagle's Medium (DMEM) supplemented with 10 % (v/v) FBS and 1 % (v/v) penicillin-streptomycin-glutamine (PSG). Cell cultures were passaged during exponential growth phase by incubating the cells with 0.05 % Trypsin-EDTA solution at 37 °C until the cells attained rounded morphology, followed by resuspension of the detached cells in their respective culture media, and sub-culturing into new sterile culture dishes or multiwell plates. All F3NC and unmodified PAA-NC suspensions were sterile filtered with a 0.2 μ syringe filter prior to use in all cell culture experiments.

Endocytosis inhibition

The internalization of FITC-labeled F3 peptides, FITC-labeled F3NCs and FITC-labeled unmodified PAA-NCs were studied separately in the MDA-MB-435 and 9L cell lines in the presence of the endocytosis inhibitors chlorpromazine (CPZ; 10 $\mu g \cdot mL^{-1}$), genistein (GEN; 200 μM) or cytochalasin D (CD; 50 μM), which block the clathrin-mediated, caveolae-mediated and macropinocytosis pathways respectively. These inhibitor concentrations were previously reported to inhibit the respective endocytic pathways *in vitro*.[74,75] Furthermore, the *in vitro* cytotoxicity of these inhibitors were tested independently by MTT assay on both the 9L and MDA-MB-435 cell lines. Concentrations higher than the abovementioned values were avoided due to cell viability issues (see Supplementary Fig. S2). All inhibitors were dissolved in DMSO as 100-fold concentrated stocks and diluted to their final concentrations in culture medium. MDA-MB-435 or 9L cells, cultured on Corning No.1½ circular glass coverslips, were incubated with either of the above inhibitors at their respective final concentrations for 30 minutes at 37 °C. Thereafter, either F3 peptides, F3NCs or unmodified (non-targeted) PAA-NCs were delivered to the cell cultures at a final concentration of 0.1 $mg \cdot mL^{-1}$ and incubated in the presence of the endocytic inhibitors for an additional 1 hour at 37 °C. Thereafter, the culture media containing endocytic inhibitors and unbound NCs were aspirated and the cells gently rinsed three times with fresh pre-warmed culture media. The cells were then labeled with Lysotracker Red DND-99 fluorophore at a final concentration of 300 nM at 37 °C for 5 minutes and washed once more prior to confocal imaging. Confocal imaging was performed on an Olympus inverted confocal microscope and all images were acquired with a 100x oil immersion objective lens. The FITC and Lysotracker Red DND-99 fluorophores were sequentially excited with the 488 nm and 568 nm lines respectively. The effects of the endocytosis inhibitors on the uptake of the F3 peptides, NTNCs and F3NCs were measured directly from the respective confocal images using ImageJ v.1.46n software. Briefly, the FITC fluorescence emission intensities were measured only within regions of interest (ROI) drawn around individual cells in each image. These ROIs were drawn so as to exclude the cell membrane, and thus any FITC fluorescence emissions from either F3 peptides or nanocarriers that were only attached to the cell membrane and had not yet been internalized. Uptake values for each inhibitor are represented as percentages of mean FITC fluorescence intensity relative to the mean of the corresponding control ±SD.

Immunocytochemistry

Immunocytochemical labeling of the membrane-bound Caveolin1, EEA1 and LAMP1 proteins was employed to study the intracellular trafficking of F3-targeted PEGylated and unmodified PAA-NCs in MDA-MB-435 cells. Cell monolayers, grown on Corning No.1½ circular glass coverslips, were treated with either unmodified PAA-NCs or F3NCs (final concentration of 0.1 $mg \cdot mL^{-1}$) for 10, 30, 60, 120, 180 and 360 minutes respectively. Following treatment, the cells were rinsed briefly three times with warm GIBCO DPBS solution and fixed in 4 % (v/v) phosphate-buffered paraformaldehyde (10 mM PBS, pH 7.2) for 10 minutes at room temperature. Immediately following fixation, the cells were subjected to three 10-minute washes with 10 mM PBS (pH 7.2) with gentle agitation on a rocking-shaker. The cells were subsequently permeabilized in permeabilization buffer (0.05 % (v/v) Tween-20, 10 mM PBS, pH 7.2) for 10-minutes at room temperature with gentle agitation on a rocking shaker, followed immediately by three washes with 10mM PBS (pH 7.2). The permeabilized cells were blocked overnight at 4°C in donkey serum buffer (10% (v/v) normal donkey serum; 0.05 % (v/v) Tween-20; 0.05 % (w/v) sodium azide; 10 mM PBS pH 7.2). Following blocking, the cells were incubated in primary antibody labeling solution (either anti-EEA1 and anti-LAMP1 or anti-Caveolin1 and anti-LAMP1 antibodies diluted 1:20 in primary antibody dilution buffer (1 % (v/v) normal donkey serum; 0.05 % (v/v) Tween-20; 0.05 % (w/v) sodium azide; 10 mM PBS pH 7.2) at room temperature in a

humidified chamber for 3 hours. Immediately following incubation, the coverslips were washed three times with PBS at room temperature (10 minutes per wash) to remove excess primary antibody. The secondary antibody incubation buffers were prepared by diluting the appropriate antibodies in a 1:500 ratio in secondary antibody dilution buffer (0.05 % (v/v) Tween-20; 0.05 % (w/v) sodium azide; 10 mM PBS pH 7.2). Incubation in secondary antibody labeling solution for 1 hour as described above for the primary antibody incubation. Following antibody labeling, the coverslips were washed three times with PBS at room temperature (10 minutes per wash) with gentle agitation on a rocking shaker. After the last wash, the coverslips were mounted (cell-surface down) onto glass slides with Dako Fluorescent Mounting Medium and stored overnight at 4 °C prior to fluorescence confocal imaging. Imaging was performed on an Olympus inverted confocal microscope and all images were acquired with a 100x oil immersion objective lens. The FITC, AF-568 and AF-647 fluorophores were sequentially excited with the 488 nm, 568 nm and 647 nm laser lines respectively.

Colocalization Analyses

All confocal images were subjected to fluorophore colocalization analysis in ImageJ v.1.64n software using the JACoP plugin.[76] Briefly, colocalization analyses were performed on a cell-by-cell basis by first drawing ROIs around individual cells in each native confocal image. Each image was then split into its component red, green and blue channels, and each ROI subsequently applied to the separated channels respectively. Thereafter, colocalization analyses between pairs of color channels (either green: FITC vs. red: Lysotracker Red/ LAMP1-AF647 or green: FITC vs. blue: EEA1-AF568/ Caveolin1-AF568) for each ROI were then performed in JACoP using automatic thresholding for each channel. Manders' M_2 coefficients based on the threshold settings were generated for each analysis, where the M_2 coefficient is defined as the fraction of the green channel (FITC) overlapping either the blue channel (EEA1/ Caveolin1) or red channel (Lysotracker Red/LAMP1). Colocalization values for each condition are based on the mean M_2 coefficients represented as percentages ±SD.

Statistical Analyses

The endocytosis inhibition and colocalization data for each cell line were statistically analyzed by One-Way ANOVA followed by Tukey's multiple comparisons test using GraphPad Prism v6.00 software for Mac OSX. In instances where selected pairs of columns in a data set were compared against each other, Bonferroni's multiple comparisons test was used in conjunction with the One-Way ANOVA test. All analyses were performed with a confidence interval set at 95 %. P-values <0.05 were considered significant.

Supplementary Material

Refer to Web version on PubMed Central for supplementary material.

Acknowledgments

The authors thank Dr. Ting Wang and Dr. Zhan Chen for their advice with regard to the experimental approach of the endocytosis inhibition study, as well as Dr. Christine Labno for her generous advice on performing confocal image colocalization analysis. The authors also thank Dr. Kathleen Nolta for her critical review of this manuscript. The authors are also grateful to the Electron Microbeam Analysis Laboratory and Microscopy and Image-Analysis Laboratory for use of their instrumentation for EM and confocal imaging. This work was supported by NIH Grants NIBIB R01 EB007977 (RK), NIBIB R000262 (RK), and NIH/NCI R33CA125297 (RK). L. Karamchand was supported by the International Fulbright Science and Technology Award and the South African National Research Foundation Doctoral Scholarship for Study Abroad.

References

1. Funkhouser J. Curr Drug Discovery. 2002:2.
2. Kelkar SS, Reineke TM. Bioconjugate chemistry. 2011; 22:1879–903. [PubMed: 21830812]
3. Harrell J, Kopelman RR. Biophotonics Int. 2000; 7:22–24.
4. Xu H, Buck SM, Kopelman R, Philbert MA, Brasuel M, Ross BD, Rehemtulla A. Israel Journal of Chemistry. 2004; 44:317–337.
5. Ross B, Rehemtulla A, Koo Y-EL, Reddy GR, Kim G, Behrend C, Buck S, Schneider R, Philbert MA, Weissleder R, Kopelman RR. Proceedings of SPIE, SPIE. 2004; 5331:76–83.
6. Kopelman R, Lee Koo Y-E, Philbert M, Moffat Ba, Ramachandra Reddy G, McConville P, Hall DE, Chenevert TL, Bhojani MS, Buck SM, Rehemtulla A, Ross BD. Journal of Magnetism and Magnetic Materials. 2005; 293:404–410.
7. Reddy GR, Bhojani MS, McConville P, Moody J, Moffat Ba, Hall DE, Kim G, Koo Y-EL, Woolliscroft MJ, Sugai JV, Johnson TD, Philbert Ma, Kopelman R, Rehemtulla A, Ross BD. Clinical cancer research : an official journal of the American Association for Cancer Research. 2006; 12:6677–86. [PubMed: 17121886]
8. Koo Lee, Y-E.; Kopelman, R. Multifunctional Nanoparticles for Drug Delivery Applications: Imaging, Targeting, and Delivery. Svenson, S.; Prud'homme, RK., editors. Springer US; Boston, MA: 2012. p. 225-255.
9. Kashyap N, Kumar N, Kumar MNVR. Critical reviews in therapeutic drug carrier systems. 2005; 22:107–49. [PubMed: 15862110]
10. Meenach, SA.; Anderson, KW.; Hilt, JZ. Safety of Nanoparticles, Nanostructure Science and Technology. Webster, TJ., editor. Springer Science+Business Media, LLC; New York, NY, USA, New York, NY: 2009. p. 131-157.
11. Soppimath KS, Aminabhavi TM, Kulkarni AR, Rudzinski WE. Journal of controlled release : official journal of the Controlled Release Society. 2001; 70:1–20. [PubMed: 11166403]
12. Gao D, Xu H, Philbert MA, Kopelman R. Nano letters. 2008; 8:3320–4. [PubMed: 18788823]
13. Wang S, Kim G, Lee YEK, Hah HJ, Ethirajan M, Pandey RK, Kopelman R. ACS nano. 2012; 6:6843–51. [PubMed: 22702416]
14. Oliveira MAM, Boyer C, Nele M, Pinto JC, Zetterlund PB, Davis TP. Macromolecules. 2011; 44:7167–7175.
15. Pinto Reis C, Neufeld RJ, Ribeiro AJ, Veiga F. Nanomedicine : nanotechnology, biology, and medicine. 2006; 2:8–21.
16. Moffat BA, Reddy GR, McConville P, Hall DE, Chenevert TL, Kopelman RR, Philbert M, Weissleder R, Rehemtulla A, Ross BD. Molecular imaging. 2003; 2:324–32. [PubMed: 14717331]
17. Sharma P, Brown S, Walter G, Santra S, Moudgil B. Advances in colloid and interface science. 2006; 123–126:471–85.
18. Selvan ST, Tan TTY, Yi DK, Jana NR. Langmuir : the ACS journal of surfaces and colloids. 2010; 26:11631–41. [PubMed: 19961213]
19. Buck SM, Koo YEL, Park E, Xu H, Philbert MA, Brasuel MA, Kopelman R. Current opinion in chemical biology. 2004; 8:540–6. [PubMed: 15450498]
20. Buck SM, Xu H, Brasuel M, Philbert MA, Kopelman R. Talanta. 2004; 63:41–59. [PubMed: 18969403]
21. Koo Lee, Y-E.; Kopelman, R. Imaging and Spectroscopic Analysis of Living Cells Optical and Spectroscopic Techniques Methods in enzymology. Conn, PM., editor. Vol. 504. UK Academic Press; 2012. p. 419-70.First
22. Moreno MJ, Monson E, Reddy RG, Rehemtulla A, Ross BD, Philbert M, Schneider RJ, Kopelman R. Sensors and Actuators B: Chemical. 2003; 90:82–89.
23. Tang W, Xu H, Kopelman R, Philbert MA. Photochemistry and photobiology. 2005; 81:242–9. [PubMed: 15595888]
24. Wang S, Fan W, Kim G, Hah HJ, Lee YEK, Kopelman R, Ethirajan M, Gupta A, Goswami LN, Pera P, Morgan J, Pandey RK. Lasers in surgery and medicine. 2011; 43:686–95. [PubMed: 22057496]

25. Tang W, Xu H, Park EJ, Philbert MA, Kopelman R. Biochemical and biophysical research communications. 2008; 369:579–83. [PubMed: 18298950]
26. Hamidi M, Azadi A, Rafiei P. Advanced drug delivery reviews. 2008; 60:1638–49. [PubMed: 18840488]
27. Oishi M, Hayashi H, Iijima M, Nagasaki Y. Journal of Materials Chemistry. 2007; 17:3720–3725.
28. Meng F, Hennink WE, Zhong Z. Biomaterials. 2009; 30:2180–98. [PubMed: 19200596]
29. Cheng R, Feng F, Meng F, Deng C, Feijen J, Zhong Z. Journal of controlled release : official journal of the Controlled Release Society. 2011; 152:2–12. [PubMed: 21295087]
30. Putnam D, Kopecek J. Bioconjugate chemistry. 1995; 6:483–92. [PubMed: 7578369]
31. Hillaireau H, Couvreur P. Cellular and molecular life sciences : CMLS. 2009; 66:2873–96. [PubMed: 19499185]
32. Rejman J, Oberle V, Zuhorn IS, Hoekstra D. The Biochemical journal. 2004; 377:159–69. [PubMed: 14505488]
33. Zhang S, Li J, Lykotrafitis G, Bao G, Suresh S. Advanced materials (Deerfield Beach, Fla). 2009; 21:419–424.
34. Yuan H, Zhang S. Applied Physics Letters. 2010; 96:033704.
35. Geng Y, Dalhaimer P, Cai S, Tsai R, Tewari M, Minko T, Discher DE. Nature nanotechnology. 2007; 2:249–55.
36. Park JH, von Maltzahn G, Zhang L, Schwartz MP, Ruoslahti E, Bhatia SN, Sailor MJ. Advanced materials (Deerfield Beach, Fla). 2008; 20:1630–1635.
37. Banquy X, Suarez F, Argaw A, Rabanel JM, Grutter P, Bouchard JF, Hildgen P, Giasson S. Soft Matter. 2009; 5:3984–3991.
38. Harush-Frenkel O, Rozentur E, Benita S, Altschuler Y. Biomacromolecules. 2008; 9:435–43. [PubMed: 18189360]
39. Perumal OP, Inapagolla R, Kannan S, Kannan RM. Biomaterials. 2008; 29:3469–3476. [PubMed: 18501424]
40. Zhang Y, Yang M, Park JH, Singelyn J, Ma H, Sailor MJ, Ruoslahti E, Ozkan M, Ozkan C. Small (Weinheim an der Bergstrasse, Germany). 2009; 5:1990–6.
41. Créancier L, Prats H, Zanibellato C, Amalric F, Bugler B. Molecular biology of the cell. 1993; 4:1239–50. [PubMed: 8167407]
42. Christian S, Pilch J, Akerman ME, Porkka K, Laakkonen P, Ruoslahti E. The Journal of cell biology. 2003; 163:871–8. [PubMed: 14638862]
43. Winer I, Wang S, Lee YEK, Lee YEK, Fan W, Gong Y, Burgos-Ojeda D, Spahlinger G, Kopelman R, Buckanovich RJ. Cancer research. 2010; 70:8674–83. [PubMed: 20959470]
44. Porkka K, Laakkonen P, Hoffman JA, Bernasconi M, Ruoslahti E. Proceedings of the National Academy of Sciences of the United States of America. 2002; 99:7444–9. [PubMed: 12032302]
45. Panté N, Kann M. Molecular biology of the cell. 2002; 13:425–34. [PubMed: 11854401]
46. Ray A, Koo Lee Y-E, Epstein T, Kim G, Kopelman R. The Analyst. 2011; 136:3616–22. [PubMed: 21773602]
47. Ray A, Lee YEK, Kim G, Kopelman R. Small (Weinheim an der Bergstrasse, Germany). 2012; 8:2213–21.
48. Wang B, Zhang L, Bae SC, Granick S. Proceedings of the National Academy of Sciences of the United States of America. 2008; 105:18171–5. [PubMed: 19011086]
49. Liu J, Kaksonen M, Drubin DG, Oster G. Proceedings of the National Academy of Sciences of the United States of America. 2006; 103:10277–82. [PubMed: 16801551]
50. Jiang W, Kim BYS, Rutka JT, Chan WCW. Nature nanotechnology. 2008; 3:145–50.
51. Yuan H, Li J, Bao G, Zhang S. Physical Review Letters. 2010; 105:1–4.
52. Hovanessian AG, Soundaramourty C, El Khoury D, Nondier I, Svab J, Krust B. PloS one. 2010; 5:e15787. [PubMed: 21203423]
53. Chen X, Kube DM, Cooper MJ, Davis PB. Molecular therapy : the journal of the American Society of Gene Therapy. 2008; 16:333–42. [PubMed: 18059369]

54. Orringer DA, Koo YEL, Chen T, Kim G, Hah HJ, Xu H, Wang S, Keep R, Philbert MA, Kopelman R, Sagher O. Neurosurgery. 2009; 64:965–71. discussion 971–2. [PubMed: 19404156]
55. Ekkapongpisit M, Giovia A, Follo C, Caputo G, Isidoro C. International journal of nanomedicine. 2012; 7:4147–58. [PubMed: 22904626]
56. Smith PJ, Giroud M, Wiggins HL, Gower F, Thorley Ja, Stolpe B, Mazzolini J, Dyson RJ, Rappoport JZ. International journal of nanomedicine. 2012; 7:2045–55. [PubMed: 22619541]
57. Legrand D, Vigie K, Said Ea, Elass E, Masson M, Slomianny M-C, Carpentier M, Briand J-P, Mazurier J, Hovanessian AG. European Journal of Biochemistry. 2004; 271:303–317. [PubMed: 14717698]
58. Pelkmans L, Bürli T, Zerial M, Helenius A. Cell. 2004; 118:767–80. [PubMed: 15369675]
59. Querbes W, O'Hara Ba, Williams G, Atwood WJ. Journal of virology. 2006; 80:9402–13. [PubMed: 16973546]
60. Hovanessian AG, Puvion-Dutilleul F, Nisole S, Svab J, Perret E, Deng JS, Krust B. Experimental cell research. 2000; 261:312–328. [PubMed: 11112338]
61. Carlsson SR, Fukuda M. Archives of biochemistry and biophysics. 1992; 296:630–9. [PubMed: 1632650]
62. Hunziker W, Geuze HJ. BioEssays : news and reviews in molecular, cellular and developmental biology. 1996; 18:379–89.
63. Janvier K, Bonifacino JS. Molecular biology of the cell. 2005; 16:4231–42. [PubMed: 15987739]
64. Huynh KK, Eskelinen EL, Scott CC, Malevanets A, Saftig P, Grinstein S. The EMBO journal. 2007; 26:313–24. [PubMed: 17245426]
65. Barel M, Meibom K, Charbit A. PloS one. 2010; 5:e14193. [PubMed: 21152024]
66. Saitoh O, Wang WC, Lotan R, Fukuda M. The Journal of biological chemistry. 1992; 267:5700–11. [PubMed: 1544942]
67. Siddiqui SF, Pawelek J, Handerson T, Lin CY, Dickson RB, Rimm DL, Camp RL. Cancer epidemiology, biomarkers & prevention : a publication of the American Association for Cancer Research, cosponsored by the American Society of Preventive Oncology. 2005; 14:2517–23.
68. Khaldoyanidi SK, Glinsky VV, Sikora L, Glinskii AB, Mossine VV, Quinn TP, Glinsky GV, Sriramarao P. The Journal of biological chemistry. 2003; 278:4127–34. [PubMed: 12438311]
69. Reyes-Reyes EM, Akiyama SK. Experimental cell research. 2008; 314:2212–23. [PubMed: 18504038]
70. Cavalli V, Vilbois F, Corti M, Marcote MJ, Tamura K, Karin M, Arkinstall S, Gruenberg J. Molecular cell. 2001; 7:421–32. [PubMed: 11239470]
71. Sorkin A, von Zastrow M. Nature reviews Molecular cell biology. 2009; 10:609–22.
72. Miaczynska M, Bar-Sagi D. Current opinion in cell biology. 2010; 22:535–40. [PubMed: 20538448]
73. Fratti, Ra; Chua, J.; Deretic, V. The Journal of biological chemistry. 2003; 278:46961–7. [PubMed: 12963735]
74. dos Santos T, Varela J, Lynch I, Salvati A, Dawson Ka. PloS one. 2011; 6:e24438. [PubMed: 21949717]
75. Gottlieb TA, Ivanov IE, Adesnik M, Sabatini DD. The Journal of cell biology. 1993; 120:695. [PubMed: 8381123]
76. Bolte S, Cordelières FP. Journal of microscopy. 2006; 224:213–32. [PubMed: 17210054]

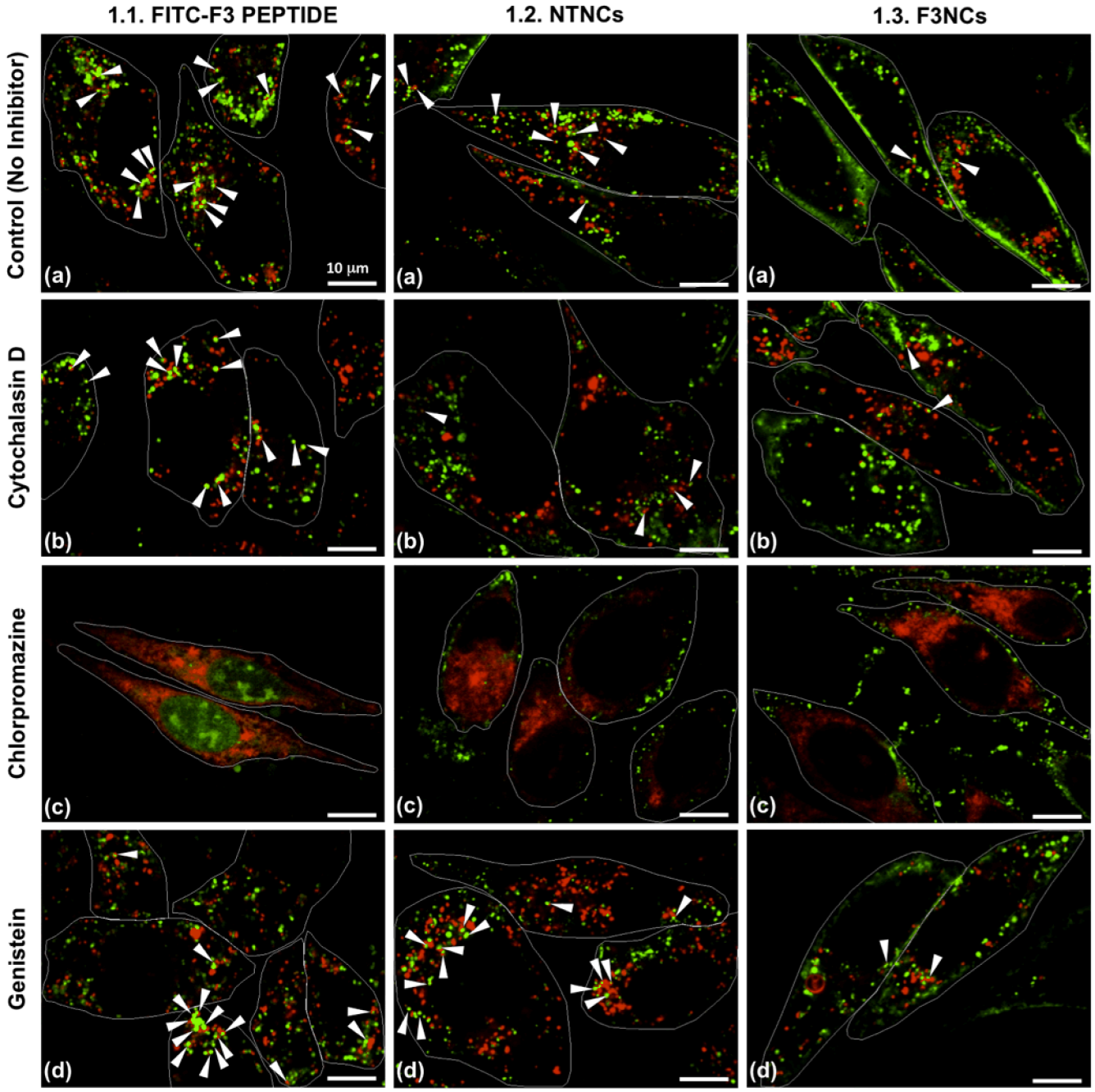

Fig 1.1–1.3.

Identification of the endocytic pathway(s) that mediate internalization of single F3 peptides (green; 1.1.a–d), non-targeted PAA nanocarriers (NTNCs; green; 1.2.a–d), and F3-targeted PAA nanocarriers (F3NCs; green; 1.3.a–d) in the 9L rat gliosarcoma cell line with the endocytic inhibitors Cytochalasin D (macropinocytosis inhibitor), Chlorpromazine (clathrin-mediated endocytosis inhibitor), and Genistein (caveolae-mediated endocytosis inhibitor). Controls constituted 9L cell cultures that received either F3 peptides, NTNCs or F3NCs in the absence of endocytic inhibitors (1.1.a, 1.2.a and 1.3.a). Lysosomes (red) were labeled with the pH-sensitive fluorophore Lysotracker DND-99. Regions of yellow/orange

fluorescence denote colocalization between lysosomes and either F3 peptides, NTNCs or F3NCs, as indicated by white arrowheads. Scale bar: 10 μm

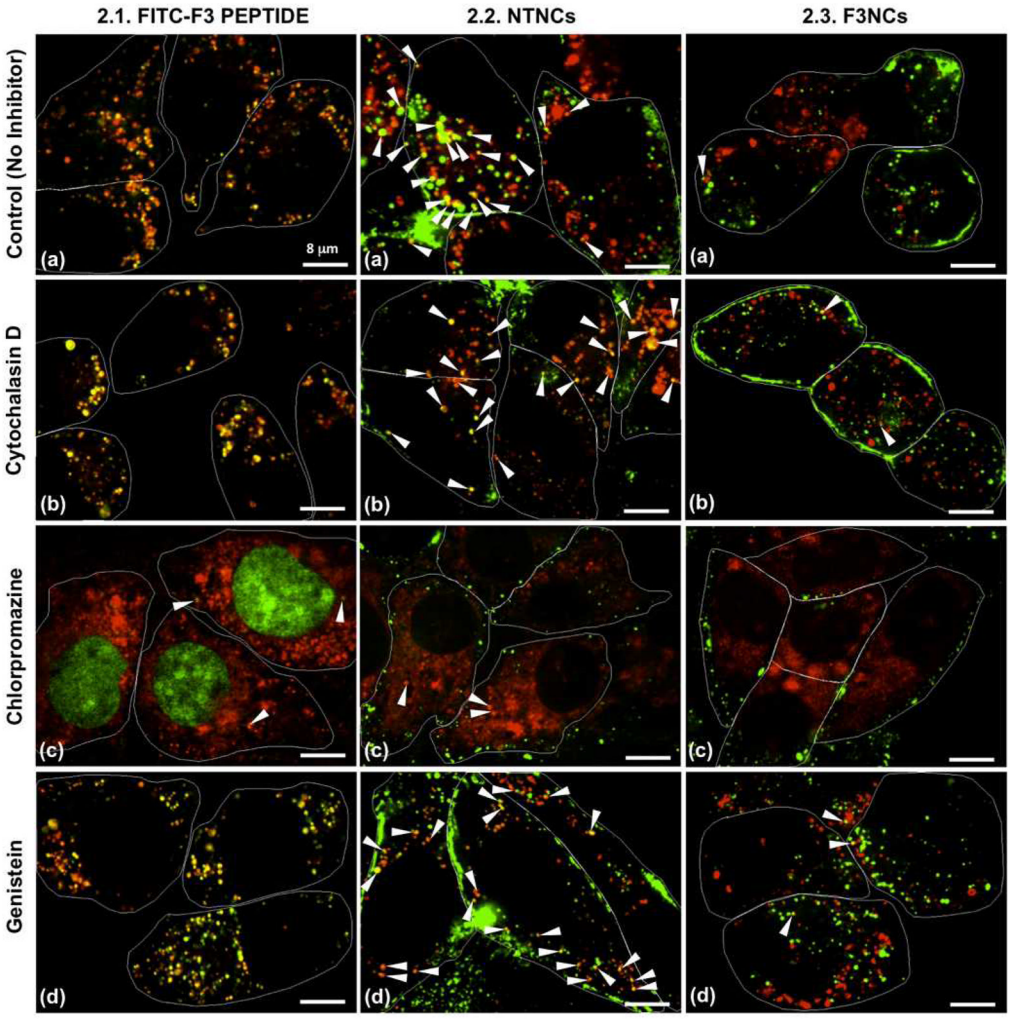

Fig 2.1–2.3.

Identification of the endocytic pathway(s) that mediate internalization of single F3 peptides (green; 2.1.a–d), NTNCs (green; 2.2.a–d), and F3NCs; (green; 2.3.a–d) in the MDA-MB-435 human melanoma cell line with the endocytic inhibitors Cytochalasin D, Chlorpromazine, and Genistein. Controls constituted MDA-MB-435 cell cultures that received either F3 peptides, NTNCs or F3NCs in the absence of endocytic inhibitors (2.1.a, 2.2.a and 3.3.a). Lysosomes (red) were labeled with the pH-sensitive fluorophore Lysotracker DND-99. Regions of yellow/orange fluorescence denote colocalization between lysosomes and either F3 peptides, NTNCs or F3NCs, as indicated by white arrowheads. Scale bar: 8 μm

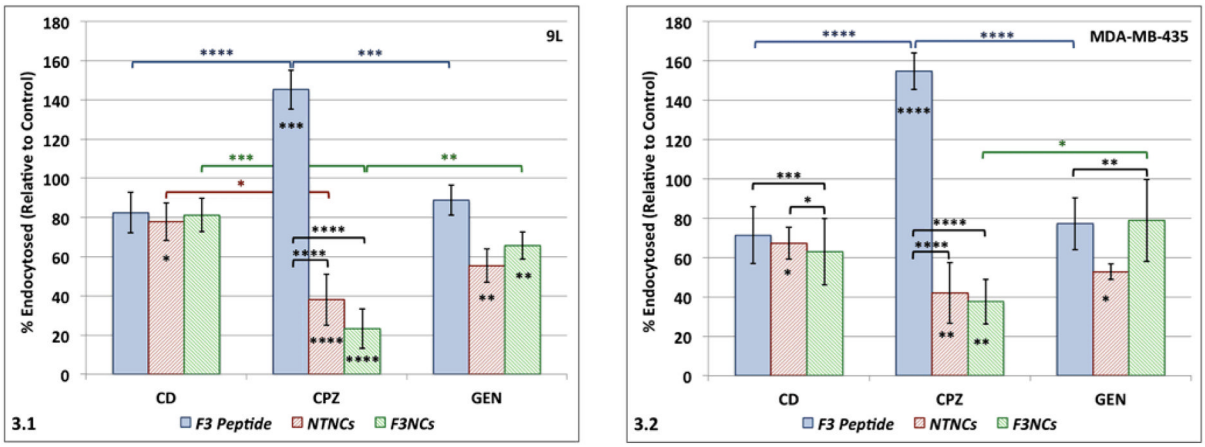

Fig 3.

Comparison of the influence of the endocytic inhibitors, Cytochalasin D (CD), Chlorpromazine (CPZ) and Genistein (GEN) on the internalization of the F3 peptides, NTNCs and F3NCs in the 9L (3.1) and MDA-MB-435 cell lines (3.2). Mean intracellular fluorescence intensities of the F3 peptides, NTNCs and F3NCs in each inhibitor treatment are expressed as percentages relative to the mean fluorescence intensities of their respective control cells, which were not treated with the inhibitors, in each cell line. Error bars show standard deviations. P-values are indicated as follows: $P<0.05$ (*); $P<0.01$ (**); $P<0.001$ (***); $P<0.0001$ (****). Brackets are color-coded to denote significant differences in uptake of F3 peptide (blue), NTNCs (red) and F3NCs (green) across different inhibitor treatments. Black brackets denote significant internalization differences between F3 peptide, NTNCs and F3NCs within the same inhibitor treatment. Asterisks indicated directly on bars denote significant difference from their respective controls (with no inhibitors).

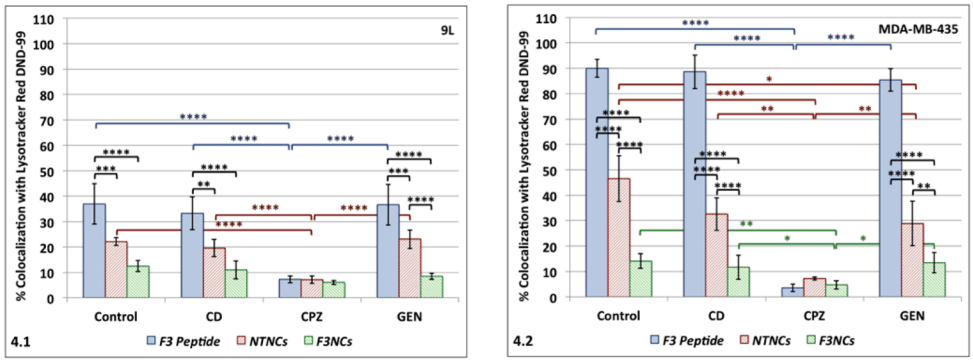

Fig 4.

Comparison of the influence of the endocytic inhibitors, CD, CPZ and GEN on the degree of colocalization of the F3 peptides, NTNCs and F3NCs with Lysotracker Red DND-99 in the 9L (4.1) and MDA-MB-435 (4.2) cell lines. All values are based on the Manders' M_2 colocalization coefficients expressed as mean percentages. Errors bars show standard deviations. P-values are indicated as follows: $P<0.05$ (*); $P<0.01$ (**); $P<0.001$ (***); $P<0.0001$ (****). Brackets are color-coded to denote significant differences in colocalization of F3 peptide (blue), NTNCs (red) and F3NCs (green) with Lysotracker Red DND-99 across different inhibitor treatments. Black brackets denote significant colocalization differences between F3 peptide, NTNCs and F3NCs within the same inhibitor treatment.

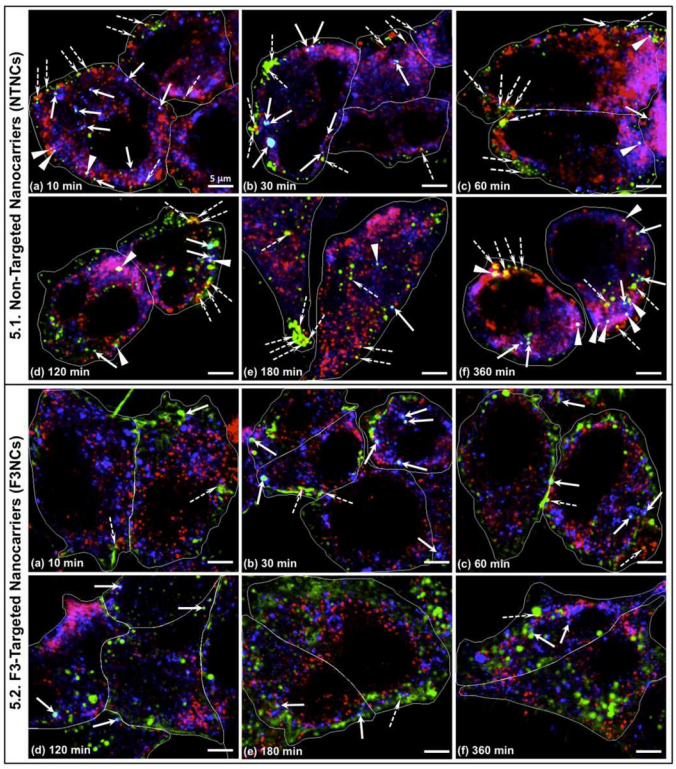

Fig 5.1–5.2.

Spatiotemporal probing of the intracellular trafficking of the FITC-labeled NTNCs (green; 5.1.a–f) and FITC-labeled F3NCs (green; 5.2.a–f) along the clathrin-mediated endocytic pathway in MDA-MB-435 cells at various time points up to 6 hours post-delivery, in relation to the early endosomes (Early Endosomal Antigen 1 (EEA1); blue) and lysosome-associated membrane protein 1 (LAMP1; red). Regions of yellow/orange fluorescence denote colocalization between LAMP1 and either the NTNCs or F3NCs (dashed white arrows), regions of light-blue fluorescence denote colocalization between EEA1 and either the NTNCs or the F3NCs (solid white arrows), and regions of white fluorescence denote colocalization between the NTNCs, LAMP1 and EEA1 (white triangles). Scale bar: 5 μm.

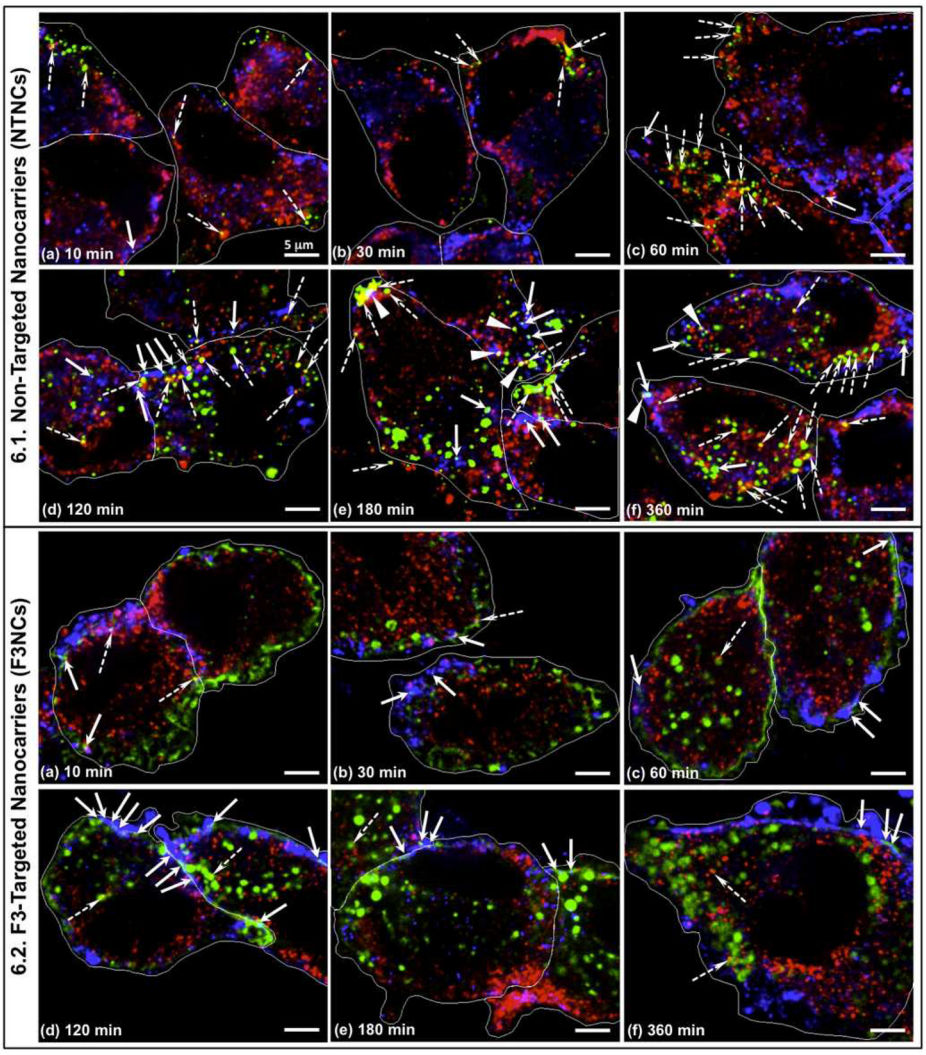

Fig 6.1–6.2.

Spatiotemporal probing of the intracellular trafficking of the FITC-labeled NTNCs (green; 6.1.a–f) and FITC-labeled F3NCs (green; 6.2.a–f) along the caveolae-mediated endocytic pathway in MDA-MB-435 cells at various time points up to 6 hours post-delivery, in relation to the caveolae (Caveolin 1; blue) and lysosome-associated membrane protein 1 (LAMP1; red). Regions of yellow/orange fluorescence denote colocalization between LAMP1 and either the NTNCs or F3NCs (dashed white arrows), regions of light-blue fluorescence denote colocalization between Caveolin1 and either the NTNCs or the F3NCs (solid white arrows), and regions of white fluorescence denote colocalization between the NTNCs, LAMP1 and Caveolin1 (indicated by white triangles). Scale bar: 5 μm.

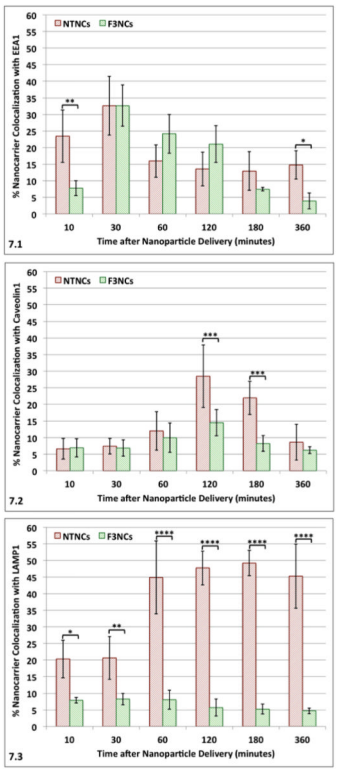

Fig 7.

Comparisons of the colocalization profiles of the NTNCs and F3NCs with EEA1 (7.1), Caveolin1 (7.2) and LAMP1 (7.3) protein markers from 10 minutes up to 6 hours post-delivery in the MDA-MB-435 cell line. All values are based on the Manders' M_2 colocalization coefficients expressed as mean percentages. Error bars show standard deviations. P-values are indicated as follows: $P<0.05$ (*); $P<0.01$ (**); $P<0.001$ (***); $P<0.0001$ (****). Black brackets denote significant colocalization differences between the NTNCs and F3NCs at the same time point.

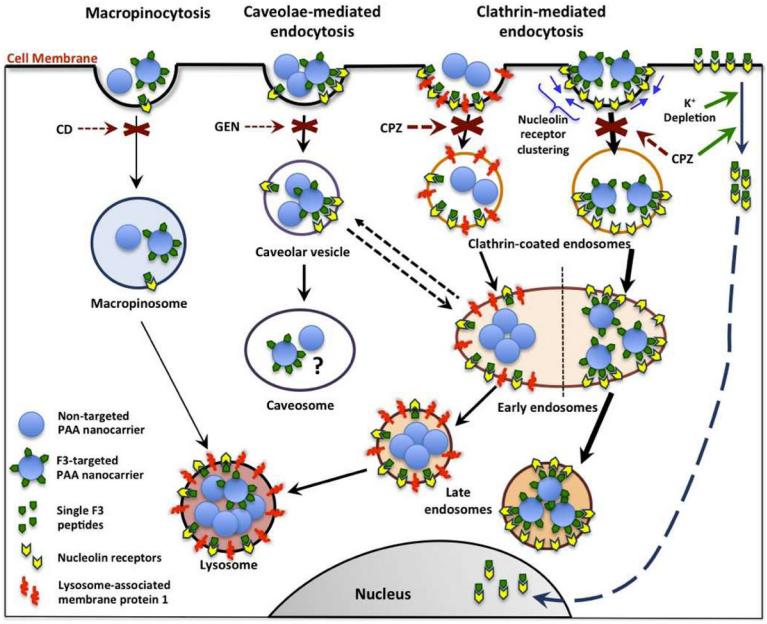

Scheme 1. Schematic summary of the endocytic pathways of internalization for F3 peptide, non-targeted and F3-targeted PAA nanocarriers (NTNCs and F3NCs) in the nucleolin-overexpressing MDA-MB-435 cell line

The F3NCs are predominantly internalized via the clathrin-mediated endocytic pathway, denoted by the potent inhibition of their internalization by Chlorpromazine (CPZ). In addition, the F3NCs employ a mechanism that circumvents their trapping within the degradative lysosomes; rather they accumulate within vesicles devoid of LAMP1 protein (Lysosome-associated membrane protein 1) in the perinuclear space. The caveolae-mediated and macropinocytosis endocytic pathways also contribute to the internalization of the F3NCs, but to a lesser extent than the clathrin-mediated pathway. In contrast, single, monovalent F3 peptides are normally trafficked to lysosomes following internalization. However, inhibition of the clathrin-mediated endocytic pathway, by both CPZ and Potassium depletion, promotes the direct translocation of F3 peptides into the nucleus. The clathrin-mediated and caveolae-mediated endocytic pathways contribute approximately equally to the internalization of the NTNCs, while macropinocytosis mediates their internalization to a lesser extent. Notably, the NTNCs co-internalize with LAMP1 proteins from the cell surface following which they are trafficked to lysosomes, as denoted by the intense colocalization between the NTNCs and LAMP1 proteins (~50%) compared to the significantly lower colocalization between the F3NCs and LAMP1 (~8%). Given the similarities observed between the MDA-MB-435 and 9L cell lines with respect to the endocytosis inhibition and Lysotracker Red colocalization profiles of the F3 peptides, NTNCs and F3NCs, this scheme also applies to the 9L cell line, and, presumably, to other cell types expressing high levels of Nucleolin on their cell membranes.